ACS OMEGA

Open Access

http://pubs.acs.org/journal/acsodf

Article

Effect of Organosilane Structures on Mineral Surface Energy and Wettability

Dany Hachem and Quoc P. Nguyen*

Cite This: *ACS Omega* 2025, 10, 15540−15552

Read Online

ACCESS | Metrics & More | Article Recommendations

ABSTRACT: The use of organosilanes has been shown to be an effective method for wettability alteration. This work explored for the first time how the structure of organosilanes impacts their ability to modify the wettability of different mineral surfaces, including pure quartz, pure calcite, sandstone, and limestone. Seven organosilanes were selected with different numbers of hydrolyzable groups, alkyl chain lengths, alkyl chain structures, and number of silicon atoms. Contact angle measurements, residual fluid saturations, and capillary pressure curves consistently showed that more hydrolyzable groups create more hydrophobic surfaces. As the number of carbon atoms increases in the silane alkyl chain, the hydrophobicity increases. The structure of the alkyl chain does not have an observable impact on the degree of wettability alteration. Finally, dipodal silanes with two silicon atoms create a much less hydrophobic surface than a single silicon atom silane. By understanding organosilane structure−property relationships with sandstone and limestone surfaces, it is possible to design tailored treatments for specific subsurface applications. Particularly in geosystems engineering, the results presented here can offer insights into enhanced oil recovery processes such as improving gas well deliverability and addressing injectivity issues during water-alternating-gas injection, as well as geological carbon sequestration processes such as improving storage capacity and caprock integrity.

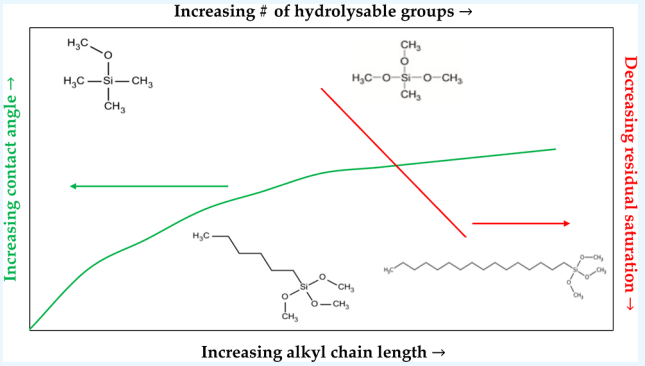

INTRODUCTION

Wettability is the tendency of a fluid to spread on a given surface. It is a characteristic of a surface that allows liquids to adhere to it. Depending on the application, surfaces are preferred to be hydrophilic or hydrophobic. Hydrophobic materials tend to self-clean and not allow contaminants to adhere strongly to them,[1] making them ideal for use in the biomedical field and manufacturing technology where anticorrosion properties are required.[2−4] Materials that are hydrophilic and oleophobic are considered efficient and cost-effective in oil−water separation processes.[5] Recent efforts have even been targeted toward the manufacturing of composite wettability surfaces to overcome the limitations of single wettability surfaces.[6] Flat, nonporous surface wettability is the subject of ongoing research in many different fields.[7] Wettability in geological porous media, however, has its own implications. In two-phase systems, the phase that tends to adhere more to the surface of the rock is called the wetting phase, and the other is called the nonwetting phase.[8] Most hydrocarbon reservoirs are thought to be originally water-wet, given that their primary composition includes quartz, carbonate, and dolomite.[9] After oil migration and depending on the composition of the rock as well as the oil, the rock wettability remains water-wet, shifts toward oil-wet, or becomes somewhere in between in a state referred to as mixed-wet or intermediate-wet. The wetting state of a reservoir influences oil production by dictating the distribution of the phases and saturation profiles before and during production.[10,11] Wettability alteration has been studied as a promising enhanced oil recovery (EOR) technique since the discovery that mixed wet core samples exhibit a lower residual oil saturation after waterflooding compared to water-wet cores.[12] The most common method of wettability alteration in the far field is the use of surfactants that adsorb on the rock and change its wetting state. Literature describing the mechanism of wettability alteration using surfactants in both sandstones and carbonates is ubiquitous.[13−16]

For unconventional reservoirs with very low permeability, hydraulic fracturing is essential for producing at a rate that is economically feasible.[17] Spontaneous imbibition experiments

Received: January 18, 2025
Revised: March 10, 2025
Accepted: April 2, 2025
Published: April 9, 2025

have shown that oil production from tight shale samples can be increased by changing their wettability to water-wet after fracturing.[18] However, the main contributor to improved production remains the injection of a slurry of water and proppants to keep the fractures open and maintain a high-conductivity channel for fluids to flow through. Typically, these proppants are designed to have specific physical properties such as grain size, weight, compressive strength, and temperature resistance.[19] The wettability of proppants has significant implications on proppant settling, oil flow performance, as well as fracture fluid clean-up. Work done with small-diameter oil-wet proppants showed strong particle suspension in monoethylene glycol solutions. Water-wet proppants of the same size exhibited substantially better settling behavior.[20] Other low-flow experiments showed that the more hydrophobic the proppants are, the lower the drag coefficient.[21] Coreflooding experiments with different proppant beds of varying wettability were conducted to determine the dependence of hydraulic fracture conductivity on proppant wettability. The beds that were more oil-wet exhibited more oil retention as determined by residual oil saturation to a waterflood, although the impact of proppant wettability was diminished at high permeability values.[22] Investigations into the factors affecting water displacement in propped fractures concluded that the wettability of the proppant has a more pronounced effect than either displacement direction relative to gravity or surface tension. Hydrophobic sand was able to achieve twice as much water displacement as the hydrophilic sand.[23] In another case, sand was treated with a hydrophobic coating that increased propped fracture conductivity by 20% below 4000 psi, with added benefits such as increased crush resistance and dust suppression.[24] More recent work compared similar-sized oil-wet and mixed-wet proppants and showed that both oil flow efficiency and water blocking inside the proppant pack were better in the mixed-wet pack.[25]

Near the wellbore, injectivity loss is an issue that adversely affects the performance of water alternating gas (WAG)-based EOR methods or CO_2 sequestration.[26] Injectivity is defined as the rate of water injection divided by the pressure difference between the injector and the producer.[27] It can be thought of as the ease with which fluids may enter the reservoir during injection in the near wellbore area. Injectivity loss, therefore, refers to the reduction of the amount of water or gas that can be injected at a given injection pressure. Since 1990, concerns have been raised about injectivity loss during WAG processes,[28] and several documented instances exist in the literature.[29−34] In brief, injectivity loss can be attributed to reservoir heterogeneity,[35] mechanical damage near the wellbore,[36,37] and reduction in water mobility due to trapped gas.[29] Most researchers focused their efforts on mitigating injectivity loss through altering the phase saturation and the interfacial tension of the injected fluids. However, there is a need for a more robust solution to the problem of gas blockage near the wellbore. This led to the investigation of wettability alteration as a possible mitigation method.[38,39] It was only in 2022 that the first investigation related to the use of silanes on rough mineral surfaces such as sandstone and limestone was conducted.[40] It was shown through contact angle measurements, centrifuge tests, capillary pressure curves, and relative permeability data from coreflooding experiments that it is possible to reduce the surface energy of the mineral surfaces to create a hydrophobic surface. The work presented here builds on these results and aims to study the structure−property relationship between different organosilane structures and mineral surfaces. It focused on the impact of organosilane type and structure on the wettability of natural rocks and associated properties such as fluid saturation and capillary pressure, which has not been found in the literature. It is clear that wettability alteration is important in many fields, particularly in subsurface engineering where its applications range from the far field to the near wellbore area. Specifically, the use of organosilanes for wettability alteration is prolific in the field of surface chemistry.[41] Their use in petroleum engineering was first reported as a way to generate oil-wet sandstone samples.[42] This investigation is the first in-depth analysis of silylating both ideal (quartz and calcite) and mineral (sandstone and limestone) surfaces using organosilanes with different structures. The parameters of interest are the number of silicone atoms, the length and type of the alkyl chain, as well as the number of hydrolyzable groups.

■ ORGANOSILANE CHEMISTRY

The general structure of the organosilanes of interest in this work is presented in Figure 1.

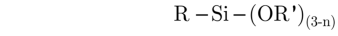

Figure 1. General structure of an organosilane.

Si is the silicon atom that is bonded to at least one alkyl group denoted as R and up to three OR′ groups called hydrolyzable groups. Bond formation proceeds according to three consecutive reactions. First, the alkoxysilane undergoes a hydrolysis reaction where the hydrolyzable groups react with water present in solution or at the surface of the substrate, as shown in the following reaction

$$R - Si - (OR')_3 + 3H_2O \rightarrow R - Si - (OH)_3 + 3R'OH$$

This reaction is relatively fast, typically occurring within minutes of the silane coming in contact with water.

The resulting silanol then condenses with itself to form a chain known as a siloxane, shown in Figure 2. The condensation reaction is relatively much slower, occurring on the order of several hours.

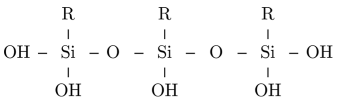

Figure 2. Hydrolyzed silane condensation into siloxane.

Finally, bond formation occurs with the hydroxyl groups present on the substrate as shown in Figure 3.

It must be noted that silane bond formation can still proceed in the absence of water through an anhydrous deposition, as shown in Figure 4. This process skips the hydrolysis and condensation reactions and is preferred when monolayer deposition is desired.

Regardless of the mechanism of silane bond formation with the surface, the resulting wettability of the surface is primarily determined by the organofunctional group R. Hydrophobic alteration is achieved when R is a nonpolar organic group such as an alkyl chain, while specific surface functionalization can be achieved when R is a halogen or an amino group.

https://doi.org/10.1021/acsomega.5c00554
ACS Omega 2025, 10, 15540−15552

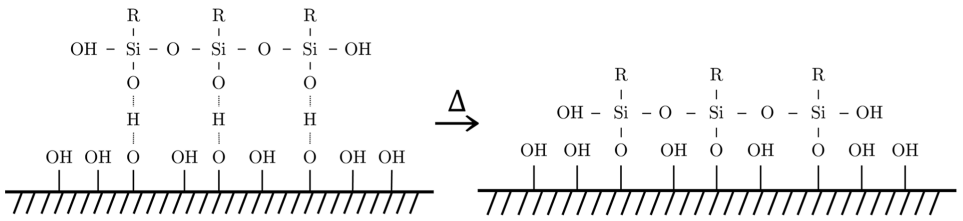

Figure 3. Silane bond formation with the hydroxylated surface.

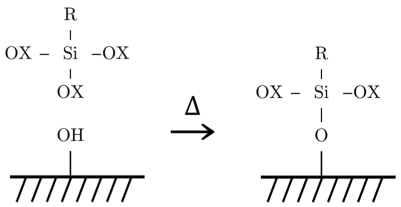

Figure 4. Anhydrous silane deposition.

MATERIALS AND PROCEDURES

Organosilanes. To study the structure−property relationship between different silane structures and mineral surfaces, seven different organosilanes were obtained from Fisher Scientific and Sigma-Aldrich. These include methyltrimethoxysilane (A), trimethylmethoxysilane (B), hexyltrimethoxysilane (C), trimethoxyphenylsilane (D), decyltrimethoxysilane (E), hexadecyltrimethoxysilane (F), and 1,2-bis(triethoxysilyl)-ethane (G). The molecular structure for each organosilane is given in Figure 5.

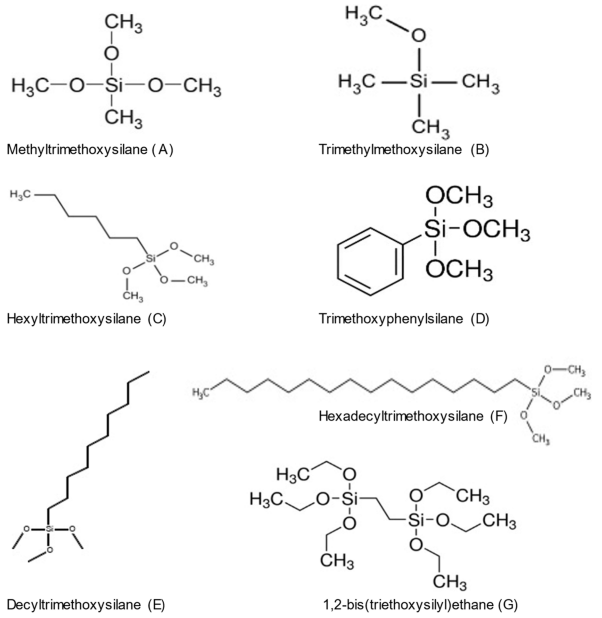

Figure 5. Molecular structure of selected organosilanes.

Mineral Surface Samples. Pure calcite and quartz samples were obtained from Ward's Natural Sciences. They were cut into 25.4 mm squares for the contact angle measurements. The samples were rinsed with iso-propyl alcohol and deionized water and then placed in an oven at 50 °C to dry for 24 h.

Outcrop Rock Samples. A Berea sandstone rock block having an average porosity of 16% and permeability of 100 mD was used to obtain sandstone outcrop samples. FTIR spectroscopy was used to determine mineralogy and showed a composition of around 90% quartz, 10% kaolinite, and trace amounts of montmorillonite and illite. An Austin Chalk rock block with an average porosity of 27% and a permeability of 10 mD was used to obtain limestone outcrop samples. FTIR mineralogy showed a composition of 98.25% calcite and 1.75% montmorillonite. For contact angle measurements, disks of 25.4 mm diameter and 5 mm thickness were cut, while for the residual fluid saturation and capillary pressure experiments, plugs with 25.4 mm diameter and 25.4 mm length were obtained. These samples were not rinsed to avoid clay swelling and were only oven-dried at 100 °C for 24 h.

Organosilane Treatment of Samples. For treating the mineral and outcrop samples used for contact angle measurement, the samples were submerged in a 0.1 wt % organosilane solution for 5 h at 50 °C to alter their wettability. These conditions were chosen because they were shown to be effective in reducing the surface energy of porous samples.[40] For the plugs used for residual fluid saturation and capillary pressure experiments, they were placed in a vacuum cell which was then filled with the organosilane solution and allowed to soak for 5 h at 50 °C.

Measurement of Contact Angles. The contact angle formed by a liquid on a solid can be measured by several techniques.[43] In this work, the water contact angles formed on the four mineral surfaces were measured using the sessile drop method. The water used contained 30,000 ppm sodium chloride (NaCl) and had a pH of 7. A model 250 goniometer/tensiometer from ramé-hart was used with a microneedle that deposited a water drop on the mineral surface, and the image analysis software ImageJ was used to measure the static contact angle. Each measurement was repeated five times to obtain a representative mean and standard deviation.

Measurement of Residual Fluid Saturation. To determine the residual fluid saturation in the outcrop plugs, a Thermo Scientific TX-200 Swinging Bucket Aluminum Rotor with Round Buckets was used. After recording the dry mass of the samples, they were placed in a vacuum cell and subjected to a 24 h vacuum treatment. For the untreated samples, the vacuum cell was then filled with brine, while the samples to be treated were filled with the organosilane solution. After soaking for 5 h at 50 °C, the treated samples were oven-dried at 50 °C until their original presoaked mass was reached. The now unsaturated samples were saturated with brine or dodecane using the same method. The fully saturated mass of the plugs was then used to determine the pore volume and porosity of the samples, as shown in Table 1. The saturated plugs were weighed and then centrifuged at 5,000 rotations per minute (RPM) for 1 h, and the residual fluid saturation was determined using a mass balance. The entire procedure was repeated three times to obtain an accurate mean and standard deviation for the measured variables.

https://doi.org/10.1021/acsomega.5c00554
ACS Omega 2025, 10, 15540−15552

Table 1. Sandstone and Limestone Plug Porosities

sandstone				limestone			
sample	dry mass (g)	pore volume (mL)	porosity (%)	sample	dry mass (g)	pore volume (mL)	porosity (%)
SU	26.95	2.19	17.0	LU	21.59	3.51	27.3
SA	25.98	2.09	16.2	LA	22.43	3.35	26.1
SB	25.44	2.06	16.0	LB	23.46	3.39	26.3
SC	25.63	2.04	15.9	LC	21.78	3.21	24.9
SD	25.88	2.11	16.4	LD	22.73	3.22	25.0
SE	26.08	2.05	15.9	LE	22.70	3.57	27.7
SF	25.79	2.04	15.9	LF	23.08	3.17	24.6
SG	25.53	2.05	15.9	LG	22.65	3.31	25.7

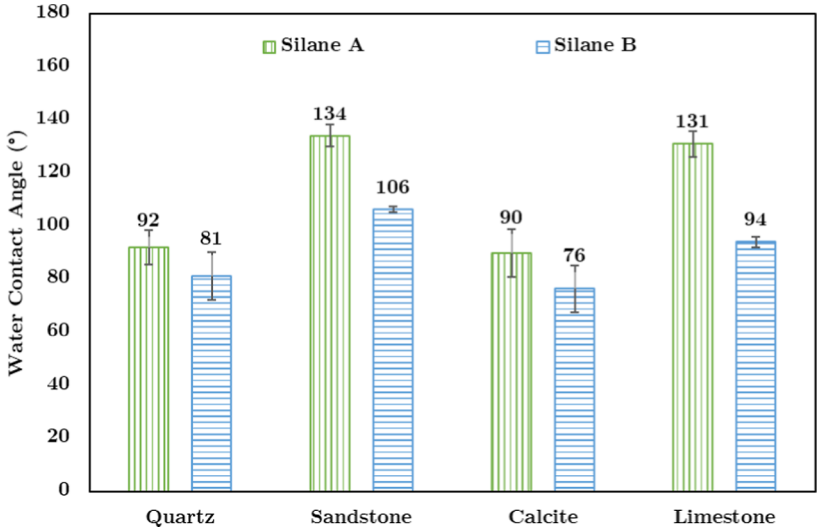

Figure 6. Contact angles of Silane A and Silane B on different surfaces.

Measurement of Capillary Pressure. The local capillary pressure can be expressed in terms of the interfacial tension (σ) between the two phases present, the contact angle between them (θ), and the pore radius of the material (r) through the Young−Laplace equation[44]

$$P_c = \frac{2\sigma\cos\theta}{r}$$

Changing the wettability of a rock can alter the capillary pressure by changing the measured fluid contact angle (θ) while keeping the interfacial tension and pore geometry constant. Thus, capillary pressure can be used to assess the effectiveness of organosilanes in altering the wettability of the sandstone and limestone plugs. The aforementioned centrifuge method can also be used to construct the capillary pressure curve for each treated sandstone and limestone sample. This process involves measuring the mass of the plug samples after 10 min of centrifuging them at a specific RPM ranging from 500 to 5,000 and determining the fluid saturation. Capillary pressure can be obtained from centrifuge data by relating fluid densities, rotation speed, and geometric properties through the following equation

$$P_c = 0.5\omega^2(\rho_w - \rho_{nw})(r_o^2 - r_i^2)$$

where ω is the rotation speed in RPM, ρ_w and ρ_{nw} are the wetting and nonwetting phase densities, which are water (1.00 g/cm^3) and air (1.27×10^{-3} g/cm^3), respectively. The geometric properties are given by r_o and r_i which are the distance from the axis of rotation to the bottom of the sample and the distance from the axis of rotation to the top of the sample, respectively.

RESULTS AND DISCUSSION

Measurement of Contact Angles. The measured water contact angles on all four mineral surfaces are shown in Figure 6. It is noted that the rough surfaces of sandstone and limestone exhibited substantially larger contact angles than their smooth ideal analogues—quartz and calcite. This is in accordance with the Wenzel model of wettability where it was first shown that the wetting properties of a rough solid are magnified as compared to a smooth surface.[45] Specifically, a hydrophilic surface will exhibit more hydrophilicity if roughened, and a hydrophobic surface will exhibit more hydrophobicity if roughened. The latter of those effects is of importance here, given that treatment with both Silane A and Silane B rendered all four surfaces significantly more hydrophobic because the initial water contact angle was zero for all surfaces. Comparing the mineralogy of silica (quartz and sandstone) and carbonate (calcite and limestone) reveals that the water contact angles are only marginally higher for the silica group. Based on the silane bond formation reaction shown in Figure 3, one would expect the silica group to have more organosilanes on its surface, given the higher concentration of hydroxyl groups. However, this was not the case, indicating that there was indeed still some adsorbed water on all four surfaces and that it was that water layer that provided the hydroxyl groups for bond formation. This is also proven by the fact that the pure calcite exhibited any

https://doi.org/10.1021/acsomega.5c00554
ACS Omega 2025, 10, 15540−15552

wettability change at all. Stable silane bonds cannot be formed on pure carbonate surfaces,[46] so it must be the case that there was some residual adsorbed water on both the calcite and limestone samples that led to the silane bonds that resulted in a more hydrophobic surface.

Number of Hydrolyzable Groups (Silane A and Silane B). The number of hydrolyzable groups and their effect on water contact angle seems more pronounced on the rough mineral surfaces than on the pure smooth surfaces. The difference between Silane A and B in their effect on water contact angle is less for quartz and calcite than for sandstone and limestone. Also, the difference is higher for the limestone than for the sandstone, which can be attributed to that the limestone samples have fewer hydroxyl groups available to react with the silanes and that Silane B has fewer hydrolyzable groups. Looking at the silane condensation reaction in Figure 2, it is clear that Silane A is able to form a siloxane chain with itself via two of the three hydrolyzed methyl groups, while Silane B cannot because of its sole methyl group. Therefore, more of the bare unreacted surface that is originally water wet is exposed to the water in the latter case, while a higher density of surface coverage is achieved with the former. In other words, surfaces treated with Silane B will have more unreacted hydroxyl groups available to attract the water molecules compared to Silane A, leading to a lower measured contact angle. Although alkyl−alkyl interactions are among the weakest intermolecular forces, they can still significantly affect material properties.[47] The intermolecular forces between two adjacent Silane B atoms prevent hydroxyl groups that are closer together from reacting with the hydrolyzed methyl group. Therefore, the apparent reduction in the ability of Silane B to generate the same hydrophobic surface as Silane A can be attributed to steric hindrance.

Length of Alkyl Chain (Silane A, Silane C, Silane E, and Silane F). The four silanes chosen for this comparison have an alkyl chain length of 1 (Silane A), 6 (Silane C), 10 (Silane E), and 16 (Silane F). Their contact angle measurements are shown in Figure 7. The percentage increase in measured water

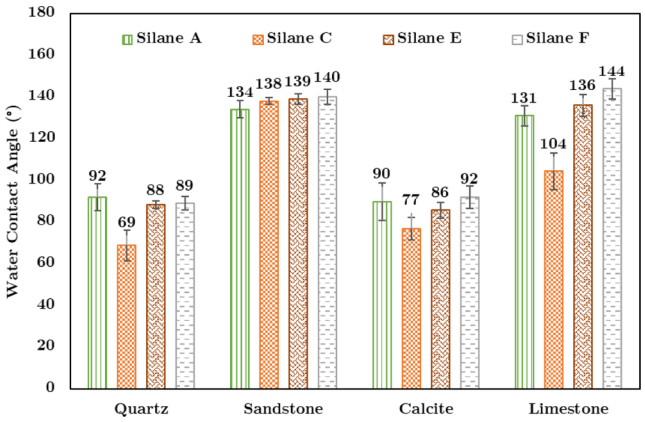

Figure 7. Contact angles of Silane A, Silane C, Silane E, and Silane F on different surfaces.

contact angles for all samples as compared to the water contact angle of Silane C (alkyl chain length of 6) is shown in Figure 8. As can be seen from these figures, there is an increase in the measured water contact angles as the length of the alkyl chain increases for all tested surfaces. Increasing the alkyl chain length from 6 (Silane C, orange checkerboard pattern) to 10 (Silane E, brown weave pattern) leads to an average increase of about 18%, and increasing it further to 16 (Silane F, gray horizontal dashes) leads to a 22% increase in the measured contact angle. Thus, it can be concluded that the impact of the increase in alkyl chain length from 6 to 16 carbons on contact angle varies significantly with different mineral surfaces (Figure 8).

The observed effect of alkyl chain length can be attributed to the increased steric hindrance with larger alkyl groups. As was shown in Figure 3, a silylated surface is shielded, allowing only the alkyl group to interact with the bulk fluid that it encounters. In the case of the silanes being compared here, the alkyl chain interacting with the water molecules is getting bulkier and bulkier as the number of carbon atoms increases, which leads to a more hydrophobic surface. This has been shown to be the case in alcohol-modified fumed silica where the treatment with *t*-butoxy alcohol led to a more hydrophobic product as compared to treatment with the less bulky and less rigid *n*-butyl alcohol,[48] and in another instance where octyl-functionalized silica nanoparticles were much more hydrophobic than methyl-functionalized nanoparticles.[49] It must be noted that the measured contact angles with Silane A (green vertical stripes) that has only one carbon atom on its alkyl chain are the same or higher than some of the other silanes with larger alkyl chains. This can also be explained by steric effects due to the anhydrous deposition of the silanes. For all the tests conducted in this work, the solvent in which the silanes were mixed was cyclohexane; therefore, the interaction with the surfaces will follow the reaction shown in Figure 4, not in Figure 3. This means that there is no formation of a condensed siloxane that reacts with the hydroxylated surface; instead, there are single silane molecules reacting with single hydroxyl groups on the surface. It can easily be seen, then, how a larger alkyl chain of a silane molecule reacting with one hydroxyl group may shield one or more adjacent hydroxyl groups from reacting with another silane molecule. This then allows some water molecules to interact with the exposed hydroxyl group, leading to more spreading and a lower measured contact angle. This is similar to the results showing that Silane B (blue horizontal stripes) exhibited lower contact angles than Silane A (green vertical stripes). Overall, it can be said that the wettability of surfaces is affected by steric hindrance that alters the molecular interactions.

Type of Alkyl Chain (Silane C and Silane D). Both Silane C and Silane D have an alkyl chain containing 6 carbon atoms, with the difference being the structure of the chain: Silane C has a straight chain that is fully saturated, while Silane D has a benzene ring. The water contact angle measurements are given in Figure 9.

The resulting water contact angles are fairly similar between Silane C (orange checkerboard pattern) and Silane D (dark-blue dotted pattern). The average difference is about 5% across the four surfaces, with some of the standard deviations being larger than that. This increases the reliability of the conclusion that the structure of the alkyl chain has no effect on the degree of induced hydrophobicity. On the molecular level, it has been shown through reversed-phase thin layer chromatography (RP-TLC) that increasing the number of unsaturated sites has a miniscule effect on the hydrophobicity of molecules.[50] Despite this, it is still possible to attribute the measured differences to the structural differences between hexane and a benzene ring. Hexane is a linear aliphatic hydrocarbon, while benzene is a planar cyclic hydrocarbon. Being a straight chain, hexane may

https://doi.org/10.1021/acsomega.5c00554
ACS Omega 2025, 10, 15540−15552

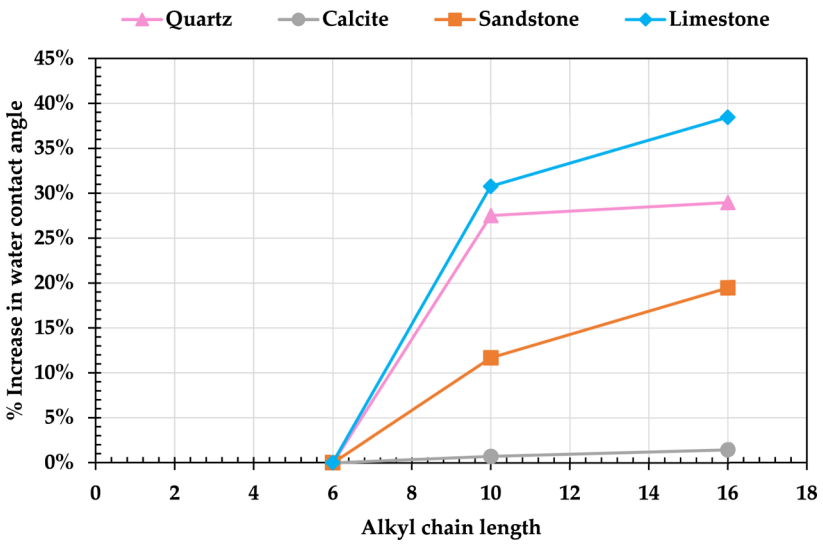

Figure 8. Percent increase of measured water contact angles compared to Silane C water contact angles.

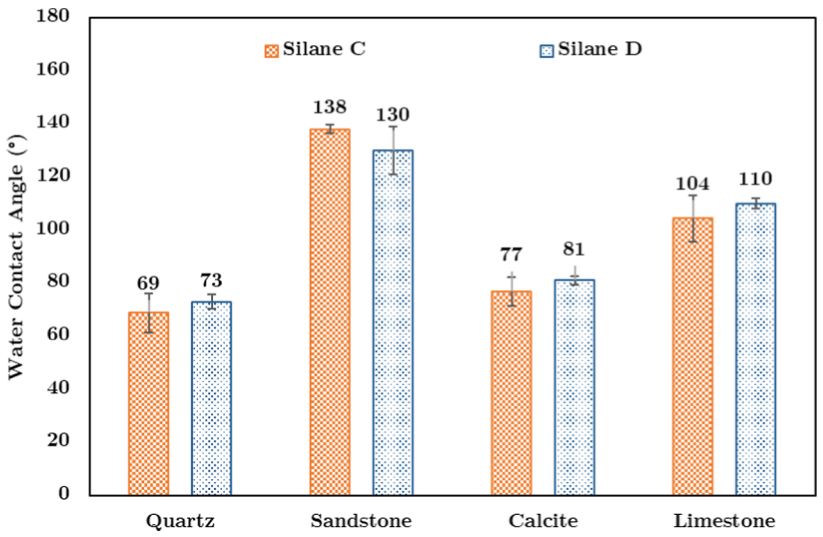

Figure 9. Contact angles of Silane C and Silane D on different surfaces.

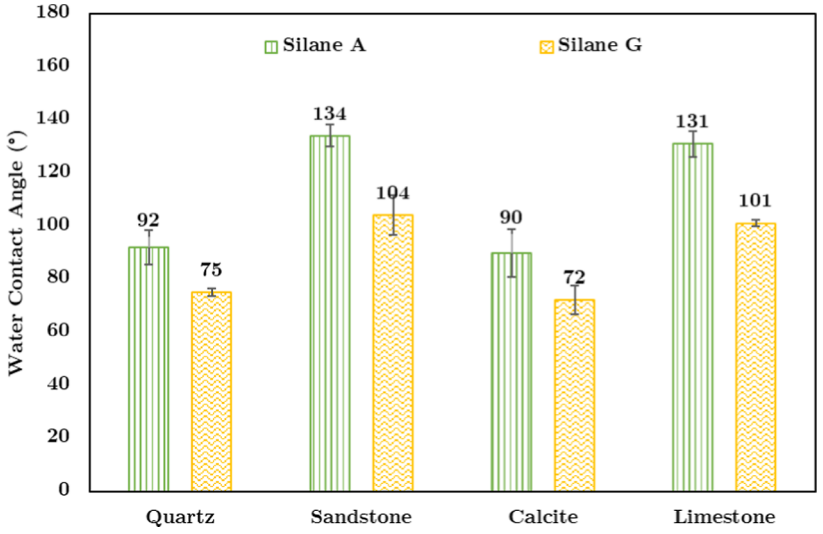

Figure 10. Contact angles of Silane A and Silane G on different surfaces.

https://doi.org/10.1021/acsomega.5c00554
ACS Omega 2025, 10, 15540−15552

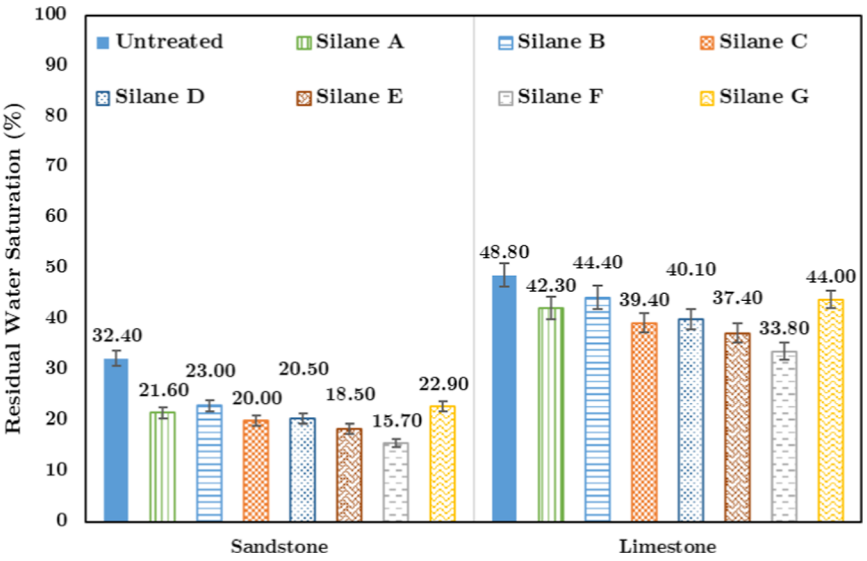

Figure 11. Sandstone and limestone residual water saturations.

have a small electric dipole moment, unlike benzene which has a perfectly symmetrical structure in which dipole moments cancel each other out. This would increase the van der Waals interactions between hexane and water, leading to a slightly more hydrophobic outcome. On the other hand, the length of hexane makes it occupy a larger surface area compared to benzene which is more compact and leads to a closer molecular packing. This, along with the delocalized electrons of the benzene ring, will enhance the dispersion forces of benzene as compared to hexane.[51] It is unclear which of these factors outweighs the others, which leads to the similar hydrophobic nature of the treated samples, as shown here by the comparable water contact angle measurements.

Number of Silicon Atoms (Silane A and Silane G). Silane G is a dipodal silane having two silicon atoms as opposed to Silane A, which is a conventional silane with only one silicon atom. The contact angle results are shown in Figure 10.

The measured contact angles for Silane G (yellow zigzag pattern) are on average 21% lower than those of Silane A (green vertical stripes) across the four tested surfaces. This is not surprising given that the two silicon atoms that are bonded to the surface are also bonded to each other as opposed to having a terminal alkyl chain extended out to interact with the water molecules. In fact, dipodal silanes were designed specifically to enhance the hydrolytic stability of conventional silanes, which undergo the hydrolysis reaction shown in Figure 2 and condense to form the siloxane rapidly. This is undesirable in certain applications as it results in phase separation and gelation.[52] Dipodal silanes also exhibit increased bond strength because of the five additional Si−O bonds they can form with the substrate. This means that the resulting silane coating is much more durable and can withstand highly acidic and brine conditions for a period of 75 days.[53] None of these properties, however, affect the interaction between the silane and the water molecules, specifically because Silane G is a "bridged" dipodal silane (terminal silicon atoms separated by a carbon chain). A "pendant" dipodal silane with a carbon chain extending out from one of the silicon atoms will indeed show more hydrophobic behavior, as it has its alkyl chain that actually can interact with the water molecules.[53] To further confirm the importance of having the alkyl chain extending out, Silane G contact angles were significantly lower than those measured with Silane C (orange checkerboard pattern), Silane E (brown weave pattern), or Silane F (gray horizontal dashes), shown in Figure 7.

Measurement of Residual Fluid Saturation. The aim of this experiment is to determine the residual fluid saturations in both the organosilane-treated and untreated (base case) rock plugs, which is the saturation at which the pore fluid loses connectivity and can no longer flow. Since this experiment requires a porous medium, only sandstone and limestone plugs were tested. Treated and untreated samples were saturated with either water or dodecane and then centrifuged to determine the residual saturations. The results for the water-saturated sandstone and limestone samples are shown in Figure 11.

The untreated sandstone sample had a residual water saturation of 32.4% after centrifuging it at 5000 rpm for 1 h. It is noted that all the silanes tested resulted in residual saturations well below the untreated case, indicating that all of them were successful in altering the wettability of the interior pore space away from water wet. Similar conclusions can be made about silane treatment of the limestone samples. As with the sandstone case, it is clear that treatment of the limestone samples with whichever silane will result in a more hydrophobic sample than the untreated sample, which resulted in a 48.8% residual fluid saturation. It is also worth noting that all residual water saturations are lower in the sandstone case than they are in the limestone case. This is due to the fact that sandstones have a much higher number of hydroxyl groups available to react with the silanes, which leads to a more uniformly hydrophobic surface and in turn leads to less fluid retention. The results from contact angle measurements on the outcrop rocks discussed above implies that the effects of organosilanes on wettability alteration are relatively smaller when applied to carbonate reservoirs.

Number of Hydrolyzable Groups (Silane A and Silane B). The sandstone sample treated with Silane A (green vertical stripes) that had three hydrolyzable groups resulted in 21.6% residual water saturation, while the one treated with Silane B (blue horizontal stripes) that had only one hydrolyzable group

https://doi.org/10.1021/acsomega.5c00554
ACS Omega 2025, 10, 15540−15552

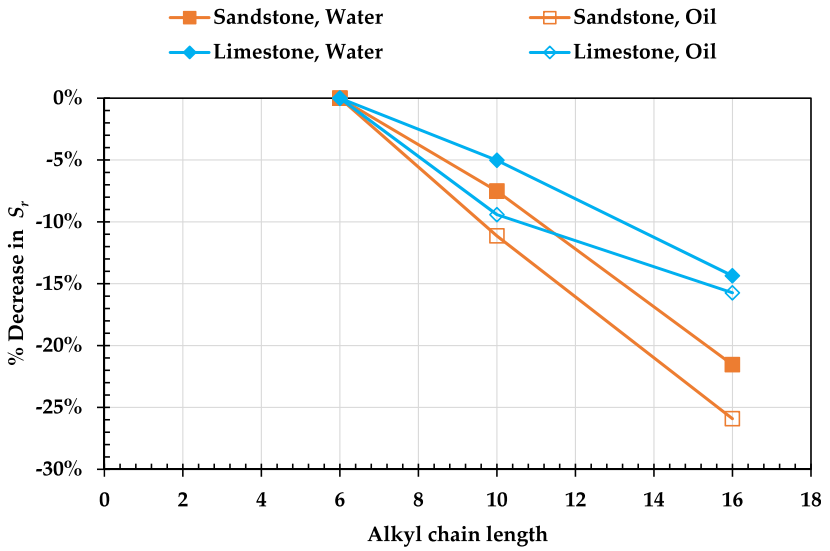

Figure 12. Percent decrease in residual fluid saturations (S_r) compared to Silane C residual fluid saturations.

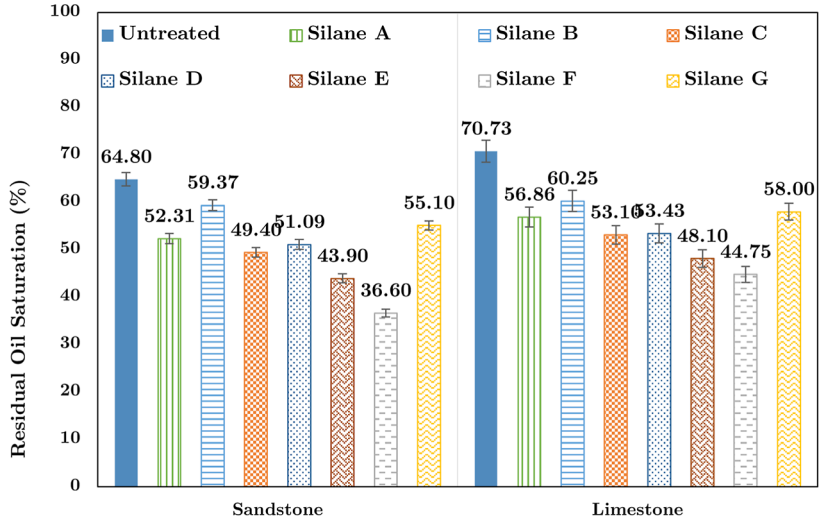

Figure 13. Sandstone and limestone residual oil saturations.

resulted in 23% residual water saturation. A comparable difference was found in the limestone samples as well, with Silane A (green vertical stripes) showing a residual saturation of 42.3% and Silane B (blue horizontal stripes) showing a residual saturation of 44.4%. There is more water remaining in the sandstone sample that was treated with Silane B compared to Silane A, indicating that the latter is more hydrophobic. This is consistent with the contact angle results shown in Figure 6 where Silane A showed higher measured contact angles. A more hydrophobic surface preferentially displaces the resident water phase that is nonwetting, resulting in a lower residual water saturation.

Length of Alkyl Chain (Silane A, Silane C, Silane E, and Silane F). Comparing the silanes of varying alkyl chain length reveals that there is a decreasing trend in the residual water saturation as the length of the carbon chain increases for both treated sandstone and limestone samples (Figure 12).

Looking at Figure 11, Silane A (green vertical stripes) with one carbon atom has a residual saturation of 21.6%, Silane C (orange checkerboard pattern) with 6 carbon atoms has a residual saturation of 20%, Silane E (brown weave pattern) with 10 carbon atoms has a residual saturation of 18.5%, and Silane F (gray horizontal dashes) with the longest alkyl chain at 16 carbon atoms has a residual saturation of 15.7% in the sandstone samples. The limestone samples show values of 42.3, 39.4, 37.4, and 33.8% for the silanes of increasing alkyl chain length, respectively. This trend is also consistent with the contact angle measurements and shows that even a small increase in the measured contact angle can lead to a significant increase in the hydrophobicity.

Type of Alkyl Chain (Silane C and Silane D). Comparing alkyl chains of the same length (6 carbon atoms) but different structures, it is clear than both Silane C (orange checkerboard pattern) and Silane D (dark-blue dotted pattern) have almost identical residual water saturations at 20 and 20.5%, respectively, for the sandstone samples and 39.4 and 40.1%, respectively, for the limestone samples. This further confirms the previously obtained contact angle measurements that despite the structural difference in the alkyl chain, the resulting hydrophobic behavior is the same.

Number of Silicon Atoms (Silane A and Silane G). The dipodal Silane G (yellow zigzag pattern) with two silicon

https://doi.org/10.1021/acsomega.5c00554
ACS Omega 2025, 10, 15540−15552

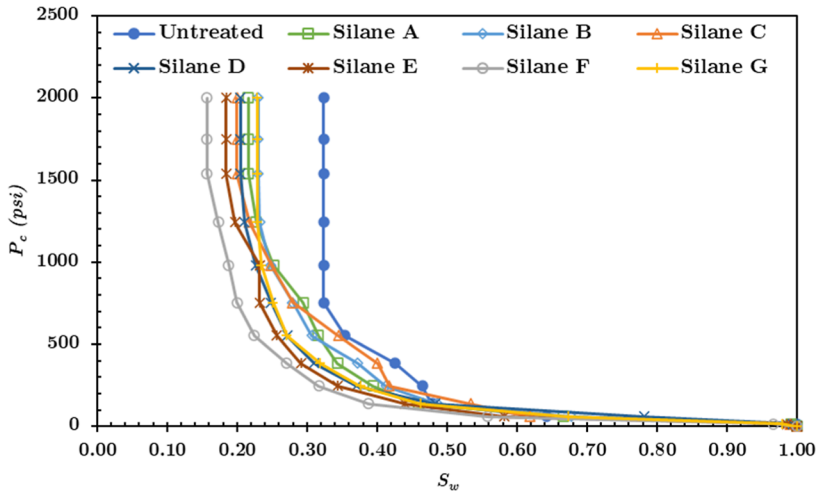

Figure 14. Sandstone capillary pressure curves.

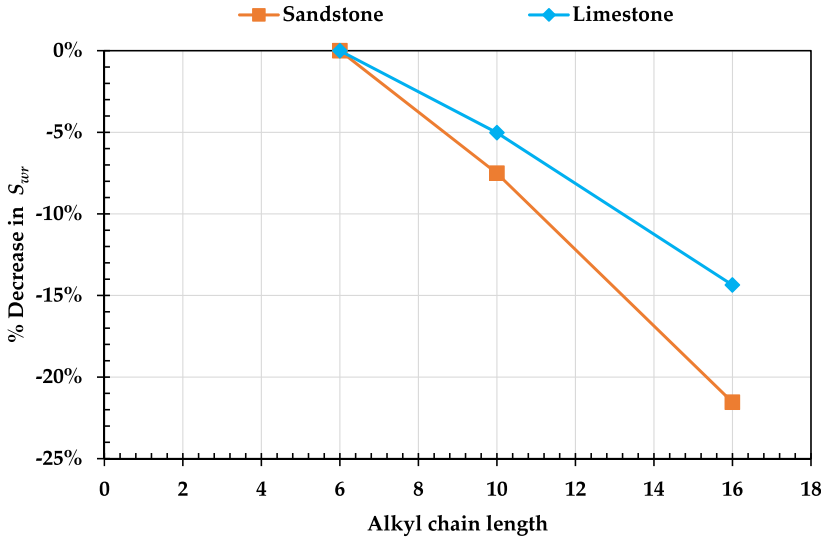

Figure 15. Percent decrease in residual water saturation compared to Silane C residual water saturation.

atoms retained more water than Silane A (green vertical stripes), with a residual water saturation of 22.9% for the former and 21.6% for the latter in the sandstone samples and 44% for the former and 42.3% for the latter in the limestone samples. As with all other results, this is consistent with the contact angle measurements which showed that the bridged dipodal silane creates a less hydrophobic surface due to the lack of an alkyl group extending out to interact with the water molecules. In the centrifuge test, this is shown by a higher residual water saturation.

The same experiment was conducted using dodecane to fill the samples, and the obtained results are shown in Figure 13.

All the residual oil saturation values for both the sandstone and limestone samples are significantly higher than the residual water saturation values. This can be attributed to the fact that when the samples are treated with silane, their surface energies decrease. As surface energy decreases, the sample transitions from water wet, oil wet, and finally to gas wet, a state where no liquid can wet the sample. Based on this notion and the results from the residual oil saturations, it can be said that treating the sandstone and limestone samples with the silanes presented here reduces the surface energy to the point where the samples are no longer water-wet, but preferentially oil-wet. This means that the sample would retain more oil than it otherwise would. Regardless, the same trends observed in the water case are observed here as shown in Figure 12: Silane B (blue horizontal stripes) with one hydrolyzable group resulted in a sample that has higher surface energy than Silane A (green vertical stripes) (i.e., more fluid retention), the increasing carbon chain length of Silane A (green vertical stripes), Silane C (orange checkerboard pattern), Silane E (brown weave pattern), and Silane F (gray horizontal dashes) resulted in lower surface energies (i.e., less fluid retention), the structural difference between the alkyl chain of Silane C (orange checkerboard pattern) and Silane D (dark blue dotted pattern) had no effect, and the dipodal Silane G (yellow zigzag pattern) resulted in much higher residual oil saturation compared to Silane A (green vertical stripes).

Measurement of Capillary Pressure. In parallel with the centrifuge test, the mass of the water-saturated sandstone and limestone samples was measured at every 500 rpm to allow the construction of a capillary pressure curve. The resulting capillary curve from the treated and untreated sandstone samples is shown in Figure 14.

https://doi.org/10.1021/acsomega.5c00554
ACS Omega 2025, 10, 15540−15552

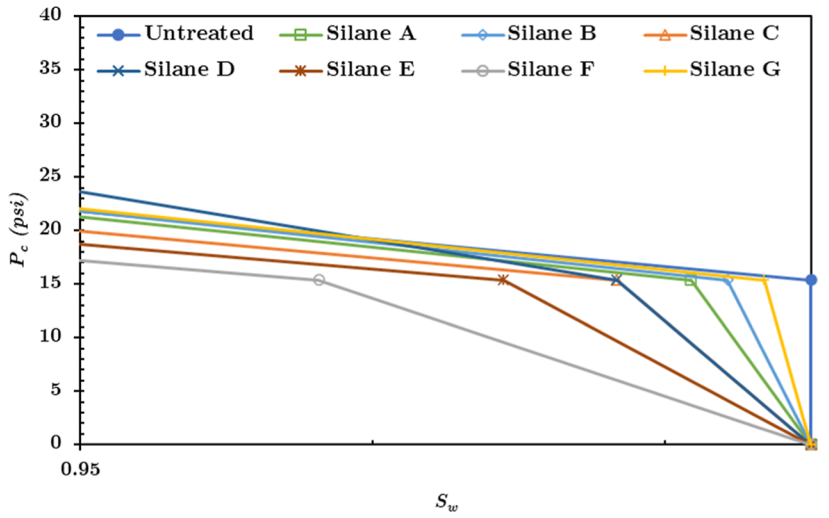

Figure 16. Early time sandstone capillary pressure curves.

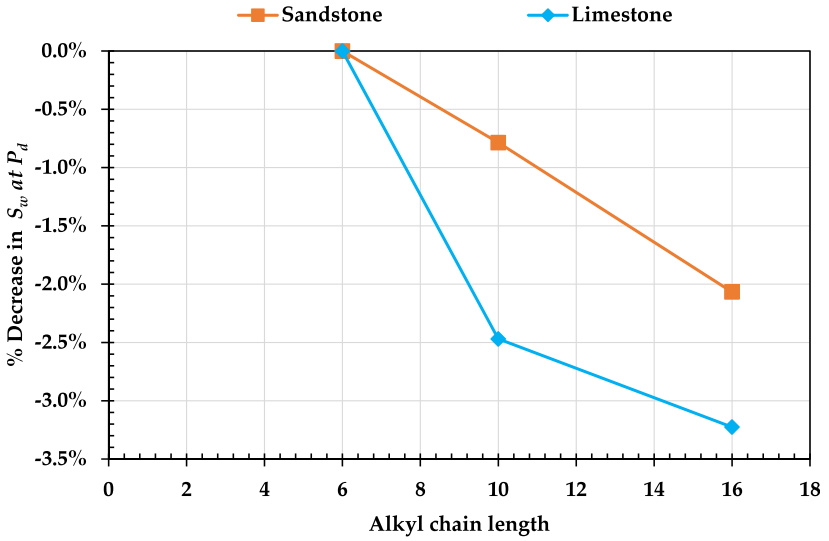

Figure 17. Percent decrease in residual water saturation (S_w) at P_d compared to Silane C.

Starting with the untreated sandstone sample (blue filled circle), it can be seen that the water saturation decreases with increasing pressure. This decrease continues until about 750 psi where the irreducible water saturation is reached, around 33%. All the capillary pressure curves for the treated samples seem to have nearly the same shape as the untreated sample but shifted to the left toward lower water saturations. This is an indication of the homogeneity of the samples and the repeatability of the results. Additionally, the shift is consistent with all the data presented so far. Silane B (blue diamond) is slightly less hydrophobic than Silane A (green square), as indicated by the higher residual water saturation at each pressure as well as a higher irreducible water saturation. Samples treated with Silane C (orange triangle), Silane E (brown star), and Silane F (gray circle) show a systematic decrease in residual water saturation in tandem with the increase in their alkyl chain length. Silane C (orange triangle) and Silane D (dark blue x) show almost identical behavior, indicating that the structural difference between their alkyl chains does not affect wettability alteration. And finally, the dipodal Silane G (yellow cross) resulted in a less hydrophobic sample than Silane A (green square), as indicated by higher water saturations at each pressure, as well as a higher irreducible water saturation at the end of the experiment. The variations of residual water saturation with alkyl chain length for the limestone and sandstone are shown in Figure 15. As the alkyl chain length increases from 6 (Silane C) to 16 (Silane F), the irreducible water saturation S_{wr} decreases.

It is also interesting to examine the pressure at which the nonwetting phase (air in this case) first enters the pore space, as shown in Figure 16.

The pressure at the onset of wetting fluid production from the sample is referred to as the displacement pressure (P_d). As the sandstone samples become less water-wet, the pressure needed to displace the resident water becomes lower. Similarly, for the same displacement pressure, a greater amount of water can be extracted. Looking at the results, it is clear that the untreated sample has a higher displacement pressure of about 15 psi. At that same pressure, the residual water saturation for Silane A (green square) is 99.2%, and for Silane B (blue diamond), it is 99.4%. For the sample treated with Silane D (dark blue x), Silane E (brown star), and Silane F (gray circle), the residual water saturations at 15 psi are 98.7, 97.9, and 96.6%, respectively. Silane C (orange triangle) and Silane D

https://doi.org/10.1021/acsomega.5c00554
ACS Omega 2025, 10, 15540−15552

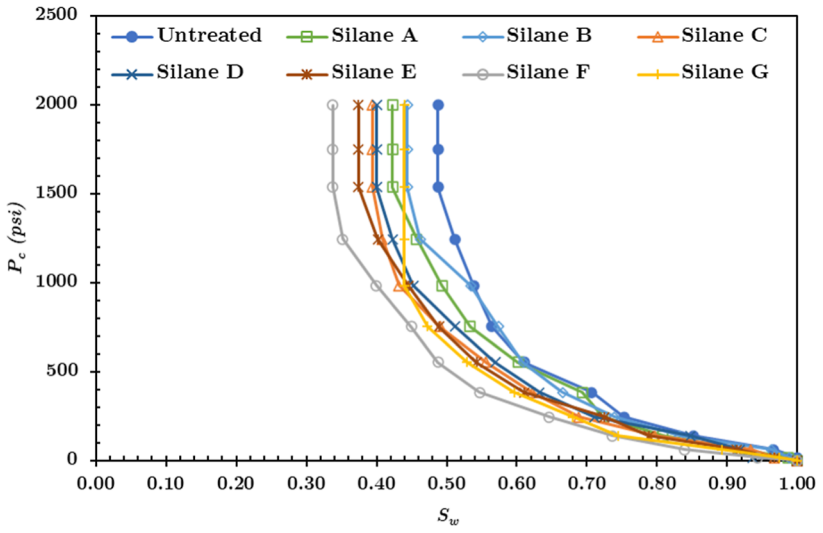

Figure 18. Limestone capillary pressure curves.

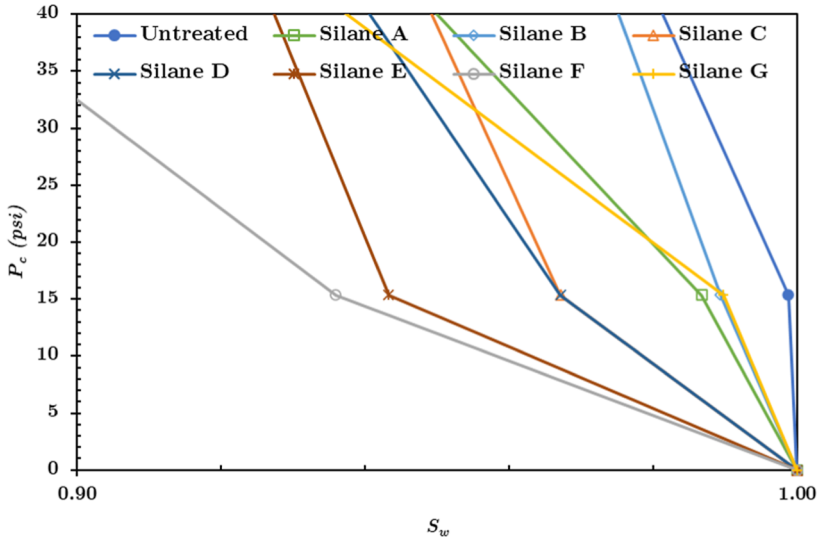

Figure 19. Early time limestone capillary pressure curves.

(dark blue x) have almost the same residual water saturation at 98.6%. Finally, Silane G (yellow cross) had a residual water saturation of 99.7% at 15 psi. Given the homogeneity of the samples, it can be said that the lower residual water saturations at the same pressure of 15 psi are an indication of a higher degree of hydrophobicity. Conversely, a lower pressure is required to reach the same residual water saturation in the more hydrophobic samples. It is clear from Figure 17 that the residual water saturation S_w decreases at the onset of fluid displacement as the alkyl chain length increases.

The same experiment was conducted using limestone samples, and the resulting capillary pressure curves are shown in Figure 18.

As with the sandstone case, the untreated limestone sample (blue filled circle) showed the highest irreducible water saturation at around 48.8%, even as the pressure went up to 2000 psi. Similarly, the treated samples showed curves that are shifted to lower water saturation. This shift means that for the same pressure, a lower residual water saturation could be achieved. It also means that the same water saturation could be achieved at lower pressures. Both indicate that the samples are moving away from the water-wet state. The same trends that were observed in the sandstone case are also present here, as well as the trends seen in the displacement pressures, as shown in Figure 19.

The residual water saturation at the displacement pressure of 15 psi was 99.9% for the untreated case (filled blue circle). For the limestone samples treated with Silane A (green square), the residual water saturation was 98.7%, while the residual water saturation for the sample treated with Silane B (blue diamond) was 98.9%, indicating the effect of three versus one hydrolyzable group. Silane C (orange triangle) with six carbon atoms on its alkyl chain showed a residual water saturation of 96.7%, the larger Silane E (brown star) with 10 carbon atoms showed a residual water saturation of 94.3%, while the largest Silane F (gray circle) with 16 carbon atoms showed a residual water saturation of 93.6%. These results validate the conclusions presented earlier that a larger alkyl chain extending out and interacting with the liquid leads to a more hydrophobic surface. Silane C (orange triangle) with the straight chain hexane alkyl group and Silane D (dark blue x) with the benzene ring both showed the same residual water

https://doi.org/10.1021/acsomega.5c00554
ACS Omega 2025, 10, 15540−15552

saturation of 96.7%. Finally, the dipodal Silane G (yellow cross) showed a 99% residual water saturation at the displacement pressure of 15 psi, slightly higher than Silane A (green square). The results shown here are in good agreement with all previously stated explanations regarding the different structures of the silanes.

CONCLUSIONS

This work explored the structure−property relationship for different silanes and mineral surfaces (quartz, calcite, sandstone, and limestone). A total of seven organosilanes were used, with an emphasis on differences in the number of hydrolyzable groups, alkyl chain length, alkyl chain type, and number of silicon atoms. Based on the results from the measurements of contact angle, remaining fluid saturation, and capillary pressure, it was concluded that the number of hydrolyzable groups does indeed affect the degree of wettability alteration as all the experiments showed that silanes with three hydrolyzable groups generated a more hydrophobic surface than silanes with one hydrolyzable group. This is because of the higher density of surface coverage that could be achieved with siloxane which would not happen if only hydrolyzable groups exist. In terms of alkyl chain length, increasing the number of carbon atoms increased the hydrophobicity of all the surfaces, with the 16-carbon silane generating the most hydrophobic surface, followed by the 10-carbon silane, and then the 6-carbon silane. Furthermore, for a fixed alkyl chain length of 6 carbon atoms, the structure of the alkyl chain did not have an effect on the wettability of the surfaces. A straight hexane alkyl chain and a benzene ring alkyl chain resulted in the same water contact angles, residual fluid saturations, and capillary pressure curves. Finally, the number of silicon atoms does have an observable effect on wettability. The dipodal silane with two silicon atoms does not have its alkyl chain extending out of the surface and interacting with the water molecules, which leads to a less hydrophobic surface than a single silicon atom silane having its alkyl chain extending out.

The results presented here offer valuable insight into the mechanism by which wettability alteration could be achieved using structurally different silanes and allow for the tailoring of surfaces to the desired degree of hydrophobicity or oleophilicity. These insights can be applied to tackle subsurface issues such as injectivity loss and proppant flow back and extend to industries beyond such as environmental remediation and corrosion resistance.

AUTHOR INFORMATION

Corresponding Author

Quoc P. Nguyen − *The University of Texas at Austin, Austin, Texas 78712-1585, United States;* orcid.org/0000-0001-9129-8700; Email: quoc_p_nguyen@mail.utexas.edu

Author

Dany Hachem − *The University of Texas at Austin, Austin, Texas 78712-1585, United States;* orcid.org/0009-0002-2082-064X

Complete contact information is available at: https://pubs.acs.org/10.1021/acsomega.5c00554

Notes

The authors declare no competing financial interest.

ACKNOWLEDGMENTS

The authors would like to thank the Chemical EOR Consortium and Gas EOR Consortium at UT Austin for supporting this work.

REFERENCES

(1) Geyer, F.; et al. When and how self-cleaning of superhydrophobic surfaces works. *Sci. Adv.* **2020**, *6* (3), 1−11.
(2) Falde, E. J.; Yohe, S. T.; Colson, Y. L.; Grinstaff, M. W. Superhydrophobic materials for biomedical applications. *Biomaterials* **2016**, *104*, 87−103.
(3) Sun, W.; Wang, L.; Yang, Z.; Li, S.; Wu, T.; Liu, G. Fabrication of polydimethylsiloxane-derived superhydrophobic surface on aluminium via chemical vapour deposition technique for corrosion protection. *Corros. Sci.* **2017**, *128*, 176−185.
(4) Chobaomsup, V.; Metzner, M.; Boonyongmaneerat, Y. Superhydrophobic surface modification for corrosion protection of metals and alloys. *J. Coat. Technol. Res.* **2020**, *17* (3), 583−595.
(5) Xu, Z.; Zhao, Y.; Wang, H.; Wang, X.; Lin, T. A Superamphiphobic Coating with an Ammonia-Triggered Transition to Superhydrophilic and Superoleophobic for Oil-Water Separation. *Angew. Chem., Int. Ed.* **2015**, *54* (15), 4527−4530.
(6) Luo, D.; Zhang, J.; Zeng, X.; Zhang, M.; Zeng, X.; Zhou, C. Fabrication and target applications of hydrophilic-hydrophobic composite wettability surfaces based on surface wettability gradient and Laplace pressure gradient regulation. *Appl. Mater. Today* **2023**, *35*, 101957.
(7) Parvate, S.; Dixit, P.; Chattopadhyay, S. Superhydrophobic Surfaces: Insights from Theory and Experiment. *J. Phys. Chem. B* **2020**, *124* (8), 1323−1360.
(8) Badawy, A. M.; Ganat, T. A. A. O. *Rock Properties and Reservoir Engineering: A Practical View*; Springer: Cham, 2022.
(9) Abdallah, W.; et al. Fundamentals of wettability. *Oilfield Rev.* **2007**, *19* (2), 44−61.
(10) Bobek, J. E.; Mattax, C. C.; Denekas, M. O. Reservoir Rock Wettability - Its Significance and Evaluation. *Trans. AIME* **1958**, *213* (01), 155−160.
(11) Morrow, N. R. Wettability and its effect on oil recovery. *J. Pet. Technol.* **1990**, *42* (12), 1476−1484.
(12) Salathiel, R. A. Oil Recovery by Surface Film Drainage in Mixed-Wettability Rocks. *J. Pet. Technol.* **1973**, *25* (10), 1216−1224.
(13) Wang, Y.; Xu, H.; Yu, W.; Bai, B.; Song, X.; Zhang, J. Surfactant induced reservoir wettability alteration: Recent theoretical and experimental advances in enhanced oil recovery. *Pet. Sci.* **2011**, *8* (4), 463−476.
(14) Mohammed, M.; Babadagli, T. Wettability alteration: A comprehensive review of materials/methods and testing the selected ones on heavy-oil containing oil-wet systems. *Adv. Colloid Interface Sci.* **2015**, *220*, 54−77.
(15) Yao, Y.; Wei, M.; Kang, W. A review of wettability alteration using surfactants in carbonate reservoirs. *Adv. Colloid Interface Sci.* **2021**, *294*, 102477.
(16) Noruzi, Y.; Sharifi, M.; Fahimpour, J.; Sabet, M.; Akbari, M.; Hosseini, S. The State-of-the-Art of wettability alteration in sandstones and Carbonates: A mechanistic review. *Fuel* **2024**, *356*, 129570.
(17) Belyadi, H.; Fathi, E.; Belyadi, F. *Hydraulic Fracturing in Unconventional Reservoirs*; Gulf Professional Publishing, 2016.
(18) Liang, T.; Zhou, F.; Lu, J.; DiCarlo, D.; Nguyen, Q. Evaluation of wettability alteration and IFT reduction on mitigating water blocking for low-permeability oil-wet rocks after hydraulic fracturing. *Fuel* **2017**, *209* (July), 650−660.
(19) Speight, J. *Handbook of Hydraulic Fracturing*; John Wiley & Sons, 2016.
(20) Soames, A.; Al-Anssari, S.; Iglauer, S.; Barifcani, A.; Gubner, R. Effect of wettability on particle settlement behavior within Mono-Ethylene Glycol regeneration pre-treatment systems. *J. Pet. Sci. Eng.* **2019**, *179* (November 2018), 831−840.

(21) Wang, L.; et al. Drag coefficient and settling velocity of fine particles with varying surface wettability. *Powder Technol.* **2020**, *372*, 8−14.
(22) Mora, T.; Orogbemi, O. A.; Karpyn, Z. T. A Study of Hydraulic Fracture Conductivity and Its Dependence on Proppant Wettability. *Pet. Sci. Technol.* **2010**, *28* (15), 1527−1534.
(23) Parmar, J.; Dehghanpour, H.; Kuru, E. Displacement of water by gas in propped fractures: Combined effects of gravity, surface tension, and wettability. *J. Unconv. Oil Gas Resour.* **2014**, *5*, 10−21.
(24) Wang, C.; Zhang, K.; O'Neil, B.; Lu, W.; Quintero, H. IPTC-18802-MS Proppant Upgrade by Wettability Alteration. *International Petroleum Technology Conference*, 2016.
(25) Dong, K.; He, W.; Wang, M. Effect of surface wettability of ceramic proppant on oil flow performance in hydraulic fractures. *Energy Sci. Eng.* **2019**, *7* (2), 504−514.
(26) Rogers, J. D.; Grigg, R. B. A literature analysis of the WAG injectivity abnormalities in the CO2 process. *SPE Reservoir Eval. Eng.* **2001**, *4* (5), 375−386.
(27) Satter, A.; Iqbal, G. M. *Reservoir Engineering: The Fundamentals, Simulation, and Management of Conventional and Unconventional Recoveries*; Gulf Professional Publishing, 2016.
(28) Gorell, S. B. Implications of Water-Alternate-Gas Injection, for Profile Control and Injectivity. *SPE Improved Oil Recovery Conference*, 1990.
(29) Schneider, F. N.; Owens, W. W. Relative Permeability Studies of Gas-Water Flow Following Solvent Injection in Carbonate Rocks. *SPE J.* **1976**, *16* (1), 23−30.
(30) Greenwalt, W. A.; Vela, S.; Christian, L.; Shirer, J. A. Field Test of Nitrogen Wag Injectivity. *J. Pet. Technol.* **1982**, *34* (2), 266−272.
(31) Grigg, R. B.; Schechter, D. S. State of the Industry in CO2 Floods. *SPE Annual Technical Conference and Exhibition, San Antonio*, 1997.
(32) Harvey, M. T.; Shelton, J. L.; Kelm, C. H. Field Injectivity Experiences With Miscible Recovery Projects Using Alternate Rich-Gas and Water Injection. *J. Pet. Technol.* **1977**, *29*, 1051−1055.
(33) Dyes, A. B.; Bensimina, A.; Saadi, A. M. A.; Khelil, C. Alternate Injection of HPG and Water - A Two Well Pilot. *Society of Petroleum Engineers of AIME, San Antonio*, 1972.
(34) Sohrabi, M.; Jamiolahmady, M. Mechanism of Injectivity Loss During Water-Alternating-Gas (WAG) Injection. *Int. Conf. on FLUID DYNAMICS & AERODYNAMICS; Corfu*, 2005.
(35) Saneifar, M.; Heidari, Z.; Linroth, M.; Purba, S. A. Effect of heterogeneity on fluid-injectivity loss during water-alternating-gas injection in the scurry area canyon reef operators committee unit. *SPE Reservoir Eval. Eng.* **2017**, *20* (2), 293−303.
(36) Pautz, J. F.; Crocker, M. E.; Walton, C. G. Relating water quality and formation permeability to loss of Injectivity. *SPE Production Operations Symposium*, 1989, pp 565−576.
(37) Harper, C.; Michael, N.; Yan, Z.; Victor, O.; Bamisebi, A. A holistic approach to injectivity decline. *SPE Nigeria Annual International Conference and Exhibition*, 2020.
(38) Arjomand, E.; Myers, M.; Al Hinai, N. M.; Wood, C. D.; Saeedi, A. Modifying the Wettability of Sandstones Using Non-fluorinated Silylation: To Minimize the Water Blockage Effect. *Energy Fuels* **2020**, *34* (1), 709−719.
(39) Arjomand, E.; Easton, C. D.; Myers, M.; Tian, W.; Saeedi, A.; Wood, C. D. Changing Sandstone Rock Wettability with Supercritical CO2-Based Silylation. *Energy Fuels* **2020**, *34*, 2015−2027.
(40) Hachem, D.; Sanders, A.; Nguyen, Q. P. Wettability Alteration Using Silane to Improve Water-Alternating-Gas Injectivity. *ACS Omega* **2022**, *7* (43), 39258−39267.
(41) Plueddemann, E. P. *Silane Coupling Agents*, 2nd ed; Plenum Press: New York, 1991.
(42) Takach, N. E.; Bennett, L. B.; Douglas, C. B.; Andersen, M. A.; Thomas, D. C. Generation of oil-wet model sandstone surfaces. *SPE International Conference on Oilfield Chemistry, Houston, TX*, 1989.
(43) Anderson, W. G. Wettability Literature Survey - Part 2: Wettability Measurement. *J. Pet. Technol.* **1986**, *38* (12), 1246−1262.
(44) Anderson, W. G. Wettability Literature Survey - Part 4: Effects of Wettability on Capillary Pressure. *J. Pet. Technol.* **1987**, *39* (10), 1283−1300.
(45) Wenzel, R. N. Resistance of Solid Surfaces to Wetting by Water. *Ind. Eng. Chem.* **1936**, *28* (8), 988−994.
(46) Shirai, K.; et al. Assessment of decontamination methods as pretreatment of silanization of composite glass fillers. *J. Biomed. Mater. Res.* **2000**, *53* (3), 204−210.
(47) Giese, M.; Albrecht, M. Alkyl-Alkyl Interactions in the Periphery of Supramolecular Entities: From the Evaluation of Weak Forces to Applications. *ChemPlusChem* **2020**, *85* (4), 715−724.
(48) Kawamura, A.; Ueno, S.; Takai, C.; Takei, T.; Razavi-Khosroshahi, H.; Fuji, M. Effect of steric hindrance on surface wettability of fine silica powder modified by n- or t-butyl alcohol. *Adv. Powder Technol.* **2017**, *28* (10), 2488−2495.
(49) Chen, W.; Karde, V.; Cheng, T. N. H.; Ramli, S. S.; Heng, J. Y. Y. Surface hydrophobicity: effect of alkyl chain length and network homogeneity. *Front. Chem. Sci. Eng.* **2021**, *15* (1), 90−98.
(50) Miura, M.; Nonomura, Y. Evaluation of hydrophobicity for fatty acids using reversed-phase thin layer chromatography. *J. Oleo Sci.* **2019**, *68* (7), 665−670.
(51) Bacon, G. E.; Curry, N. A.; Wilson, S. A. A crystallographic study of solid benzene by neutron diffraction. *Proc. R. Soc. London, Ser. A* **1964**, *279* (1376), 98−110.
(52) Zazyczny, J.; Arkles, B. Dipodal Silanes. *Adhes. Sealants Ind.* **2008**, *15* (11), 33−35.
(53) Singh, M. P.; Keister, H. K.; Matisons, J. G.; Pan, Y.; Zazyczny, J.; Arkles, B. Dipodal silanes: Important tool for surface modification to improve durability. *MRS Online Proc. Libr.* **2014**, *1648* (4), 1−7.

https://doi.org/10.1021/acsomega.5c00554
ACS Omega 2025, 10, 15540−15552